Impacts of Emergent Vegetation on Hyporheic Exchange

S. Huang[1,2], and J. Q. Yang[1,2]

[1] Saint Anthony Falls Laboratory, University of Minnesota, Minneapolis, MN 55414.

[2] Department of Civil, Environmental, and Geo-Engineering, University of Minnesota, Minneapolis, MN 55455.

Contents of this file

Introduction

This supporting information contains Text S1-S4, Figs. S1-S12, and Table S1. In Text S1, the procedure to make hydrogel beads used in the experiments is briefly summarized. Text S2 provides details of dye calibration. Image processing steps that were used to calculate the washout curves and the fitting process of the proposed model are described in Text S3. Text S4 discusses the results of experiment with a side-looking camera.

Fig. S1 is the schematic diagram of the proposed model.
Fig. S2 shows the diagram of the flume.
Figs. S3 and S4 are images show the process to make hydrogel beads.
Fig. S5 shows the location of velocity measurements of the cases with vegetation.
Fig. S6 shows the results of dye calibration.
Figs. S7 and S8 show the injection equipment and dye injection locations.
Fig. S9 shows the snapshots of the sediment bed at different times.
Fig. S10 describes the imaging processing steps.
Fig. S11 shows the results of the experiments with a side-looking camera.
Fig. S12 compares the effective diffusion coefficients of cases without vegetation with the previous study.
Table S1 lists the flow conditions of each case.

Text S1.

The hydrogel beads were made following the procedure proposed by Ma et al. (2019). First, sodium alginate (Sigma-Aldrich W201502) and gellan gum (Sigma-Aldrich P8169) were mixed with deionized water, and their final concentrations were 0.24 wt% and 0.96 wt%, respectively. To make sodium alginate and Gellan Gum fully dissolve into the water, the gel solution was autoclaved with the liquids cycle (sterilization temperature: 121 °C, sterilize time: 30 minutes). After cooling down at least 12 hours, the polymer solution was dropped into 10 mM magnesium chloride solution ($MgCl_2$, Millipore 442611-M) through plastic tubes (4 mm I.D.), as shown in Fig. S3. The magnesium ions cause sodium alginate and gellan gum to cross link and form discrete spherical hydrogel beads (Fig. S4). The diameters of the hydrogel beads are 5.6±0.6 mm.

Text S2.

Two calibration tests were performed to confirm the linear relationship between the dye concentration in the sediment and the fluorescence intensity detected by the downward-looking camera. First, we placed an 8-cm-square box filled with beads and known concentrations of fluorescent dye under the mesh in flume filled with water. We illuminated the dye and hydrogel beads in the box with the blue LED lamp and measured the averaged fluorescence intensity of the emitted green light using the downward-looking camera with a green light filter. Because the beads are transparent, the image intensity detected by the downward looking camera represents the accumulative signal of fluorescence emitted by the dye at different depth. The results are shown in Fig. S6a. Our measurements show that the fluorescence intensity is linearly proportional to the accumulative dye concentration, or mass of dye per unit area, and the thickness of the beads does not affect the detected fluorescence intensities.

Second, we inject 5 mL of dye with concentration of 0.5, 1.0, 1.5 or 2.0×10^{-4} wt% into the sediment up to 5 cm deep at the same location within 10 seconds for all cases. The image of the sediment bed was taken by a downward-looking camera. A binary image mask was used to block the image outside the dye plume, and the pixels on the dye plume was identified by the procedure mentioned in Text S3. Finally, the florescence intensity detected by a downward-looking camera are calculated by averaging the image intensity of pixels on the dye plume. The results show that the relationship between fluorescence intensity and injected dye concentration is linear (Fig. S6b), suggesting that the fluorescence intensity is linearly related with dye concentration in the sediment. Note that because the dye was injected at the same location with similar flow rate (~0.5 mL/s), the dye plume volume and location of dye plume in the sediment is similar between cases, and dilute effect caused by transparent sediment is similar in the calibration tests. The injected volume 5 mL is the same with the volume of the dye injected in the dye release experiments at one location and 2.0×10^{-4} wt% is the initial concentration used in the experiments.

Text S3.

Here we describe the imaging processing steps to calculate the fluorescence intensity in the sediment from images shown in Fig. S9. First, the recorded images were cropped to an area contain several repeated patterns of vegetation dowels, and the area occupied by and near the vegetation dowels was removed. Second, the normalized histogram of intensity of remaining pixels was fitted by the sum of the probability density functions of two normal distributions (Fig. S10c). Based on the histograms, the pixels were classified into two categories: (i) pixels occupied by the mesh were identified as the pixels with intensity histogram following the distribution with lower mean intensity and (ii) pixels occupied by hydrogel beads and pore water were identified by pixels with intensity histogram following the distribution with higher mean intensity. Note that for consistency, the number of pixels belong to the two histograms were kept at 60:40 ratio.

To estimate the spatial variation of the hyporheic exchange, the analyzed area was further divided into four subregions. In each subregion, fluorescence intensity of the sediment was estimated by averaging the image intensity of pixels occupied by the hydrogel beads and pore water. From the series of images, four washout curves were obtained in each test. Two of the examples are shown in Fig. 2.

After we obtained the curves of fluorescence intensity versus time, we fitted the curves with the solution of the first order equation (Eq. 1). The background image intensity and the effective hyporheic exchange velocity V_H were chosen as fitting parameters. The fitting procedure includes two steps. First, we determined the duration when the streamwise fluorescence intensity decreases uniformly. The fluorescence intensity of original analyzed region was averaged in spanwise direction. Then, the resulting streamwise profiles were normalized by the profile at different times. If the slope of the normalized profile was not statistically different from zero, the normalized profile was horizontal, indicating that the fluorescence intensity decreases uniformly in streamwise direction (Fig. S11d). We fitted the model to the data during this time because the decrease in fluorescence intensity was mainly contributed by the leaving of dye from the sediment (Text S4). Secondly, the first order equations were solved numerically, and the fitting parameters were determined by minimizing the root mean square error between the simulated curve and measured curve from each subregion. Here the root mean square error was calculated by subtracting the linearly interpolated values of the simulated curve at the time when the images were taken. The background image intensity was first determined by fitting the whole washout curve with the solution of Eq. 1. Then, the effective hyporheic exchange velocity V_H were determined by fitting the measured fluorescence intensity when the streamwise fluorescence intensity decreases uniformly. The code of the image process and the model fit can be found on Zenodo (https://doi.org/10.5281/zenodo.6407198).

Text S4.

Dye release experiments with a side-looking camera were conducted to illustrate the vertical and streamwise migration of the dye plume in sediment bed (Fig. S11a). The solid fraction of vegetation is 0.05, and the velocity of overlying flow is 3.6 cm/s. Figs. S11b and S11c shows the distributions of fluorescence intensity in vertical and streamwise directions (along z-axis and x-axis), respectively. Fig. S11b shows that the region where fluorescence intensity exceeds 80% peak fluorescence intensity (between gray dash lines) does not expend during the first 2 hours of the experiment, suggesting the vertical migration of dye through the sediment is not significant. For the streamwise elongation of dye plume, the velocity of the dye front is 1.0~1.5% of the velocity of overlying flow to the downstream in the sediment. We noticed that the streamwise fluorescence intensity decreases uniformly when $t = 0.3$-2 hours (Fig. S11d). It implies that the dye fluxes entered and leaved the analyzed area were similar in the sediment and the decrease in fluorescence intensity captured by the downward-looking camera was mainly due to the exchange of dye to the surface water. We fitted the data with the proposed model when the fluorescence intensity decreases uniformly to quantify the hyporheic exchange across the sediment-water interface.
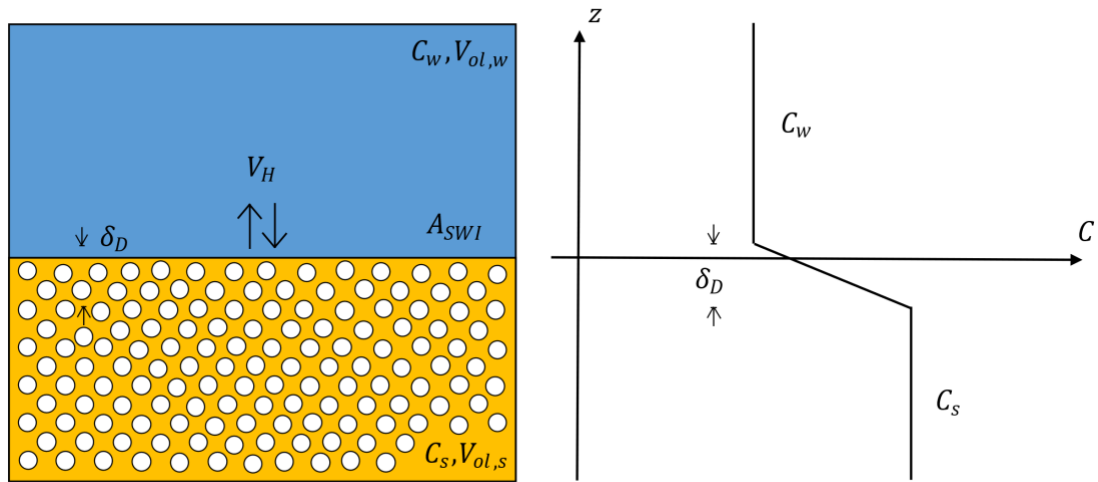
Figure S1. Schematic diagram of the proposed model. The blue and yellow area indicate the surface water and pore space in the sediment bed, respectively. C_w and C_s denotes the concentration of a solute in surface water and pore water within the sediment, respectively.
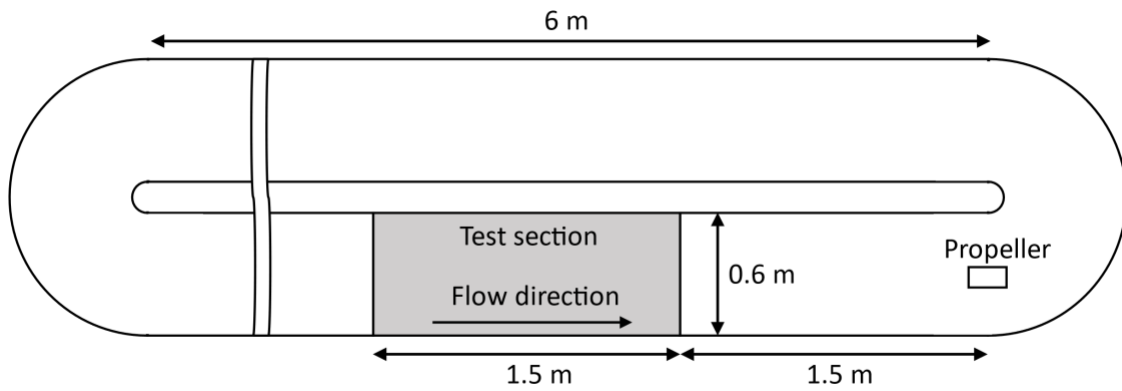

Figure S2. Schematic diagram of the race-track flume with a horizontal bed. The propeller was used to drive the flow.

Figure S3. The dropping system used to make hydrogel beads with controlled size. The polymer solution was poured into the cups and dropped into the 10 mM magnesium chloride solution in the container blow.
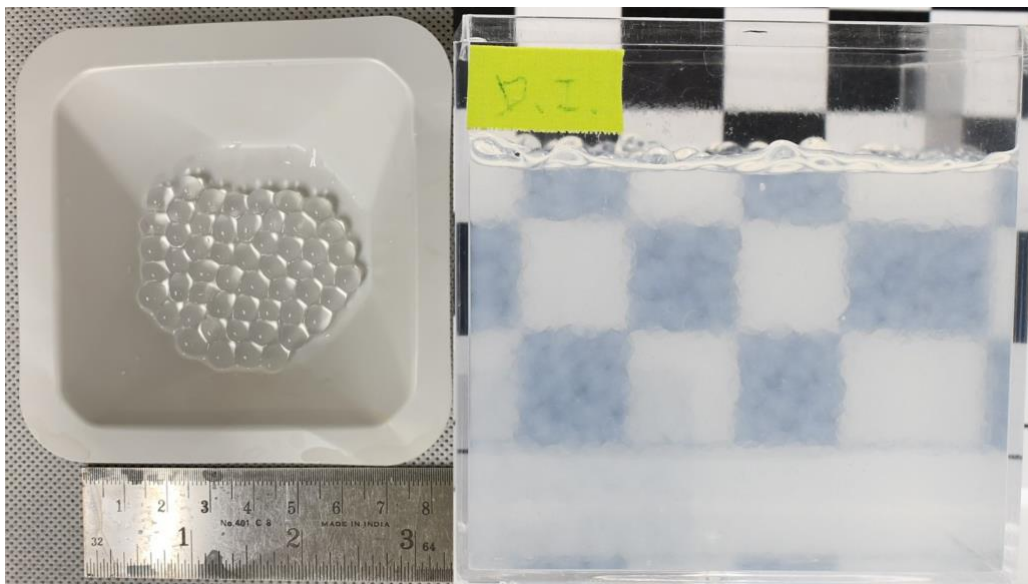
Figure S4. The hydrogel beads. The width of the container filled with hydrogel beads and water is 8 cm.
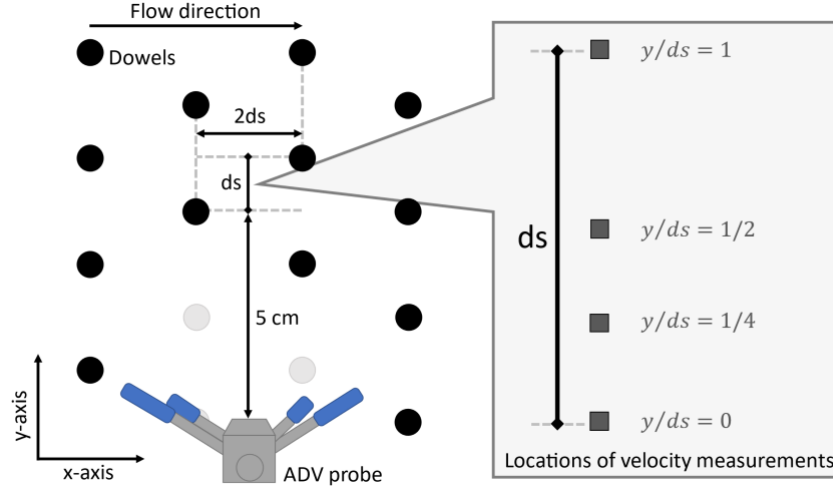
Figure S5. The locations of the velocity measurements for the vegetated cases using a side-looking Acoustic Doppler Velocimetry (ADV) in a flume with dowels (top view). The black circles represent vegetation dowels. The lateral center-to-center distance between two dowels $2ds = 2.6$ cm. The square symbols indicate the locations of the velocity measurements relative to the vegetation dowels. Three dowels were removed to make space for the ADV probe (gray circles). The wake zones of the ADV probe did not affect the flow at measured locations. The measurements were taken at 64.0 cm downstream of the leading edge of the vegetation patch (in the middle of the test section). The vertical measured interval of each profile is 2.5 mm under 4 cm depth and 2-3 cm for the rest of the water depth. The distances between measured points and side wall are 300.0, 303.5, 307.0, and 314.0 mm, respectively. The spatially averaged velocity and the near-bed k_t was calculated using a spatial-average method justified in Yang et al. (2015) from local velocity and k_t at 4 locations. Specifically, the measurements at $y/ds = 0$, 1/4, 1/2, and 1 were weighted based on the lengths they cover along the transect of length ds, which are 12.5%, 25.0%, 37.5% and 25.0%, respectively. Yang et al. (2015) showed that the measurements at 4 representative locations relative to the upstream dowel are sufficient to obtain a converged result in channel with same model vegetation presented here. We further support this observation by showing that the differences between the mean flow velocity calculated from five profiles and four profiles are less than 5%.
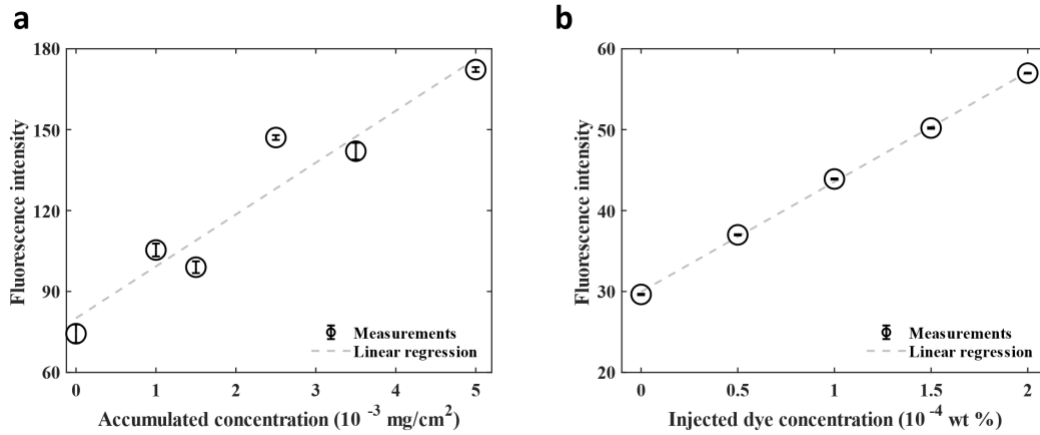

Figure S6. The linear relationship between injected dye concentration and fluorescence intensity detected by the downward-looking camera. (a) Dye calibration with a plastic box. The dashed line

6

represents the linear fit $y = 19.2x + 80.0$ with $R^2 = 0.91$. (b) Dye calibration with dye injection. The dashed line represents the linear fit $y = 13.6x + 30.0$ with $R^2 = 0.99$.
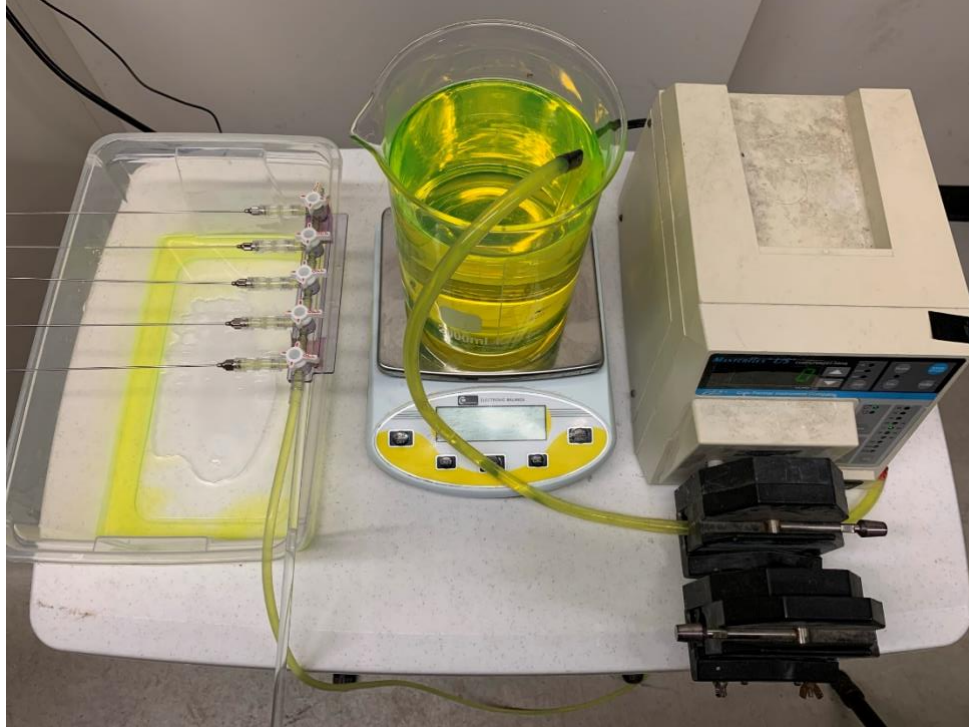

Figure S7. The dye injection equipment. A diverter was attached to five needles and a peristaltic pump. The amount of dye injected at each location was monitored by a scale during the injection process. Afterward, the total amount of injected dye was calculated from the weight of dye solution in the container before and after the dye injection.
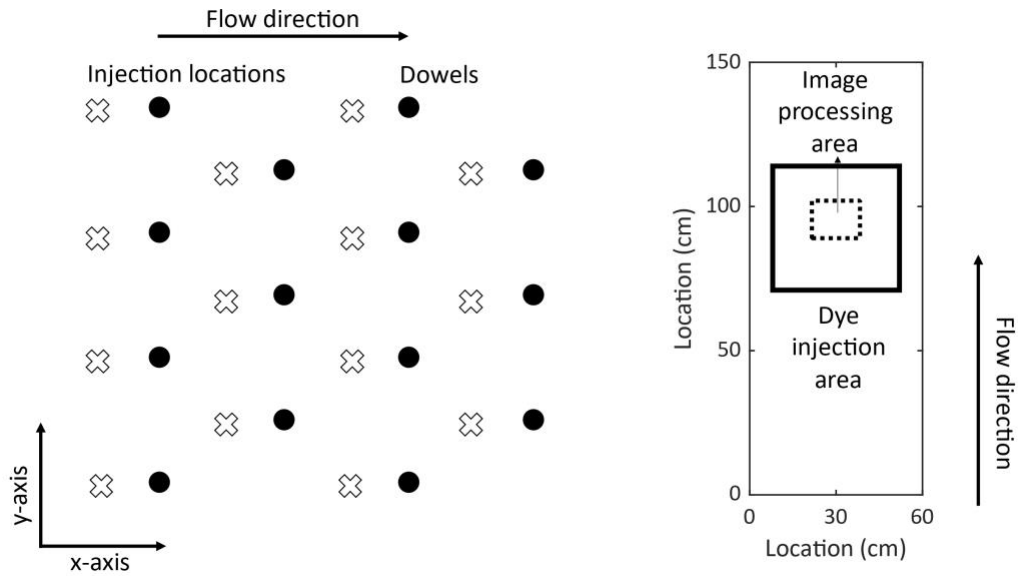
Figure S8. Location of dye injection. The left figure shows the dye injection locations relative to the dowl positions. The figure at right hand side shows the dye injection area (44 cm × 43 cm, thick solid line) in the test section and a smaller image processing area (22 cm × 17 cm, dash line).

$t = 0\,\text{h}$ $t = 1\,\text{h}$ $t = 4\,\text{h}$ $t = 17\,\text{h}$
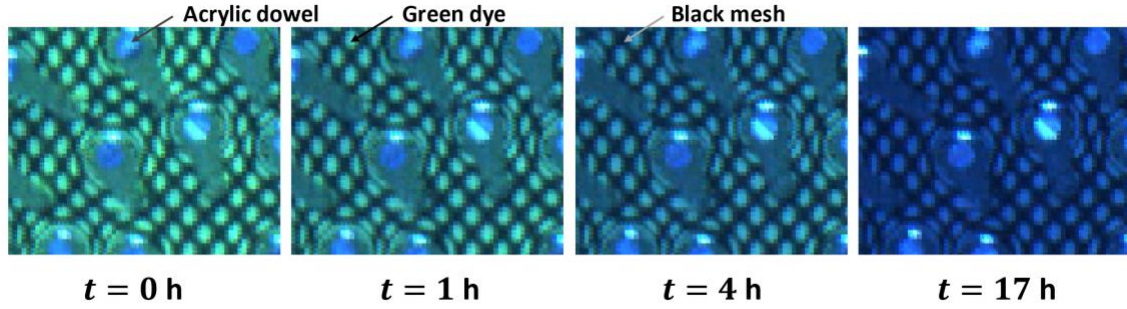
Figure S9. Images showing the decrease in the concentration of a fluorescent dye in the sediment over time during a dye release experiment. The dye, illuminated by a blue light lamp, emitted green light. The mean flow velocity of this case is 0.7 cm/s. Flow was started at $t = 0\,\text{h}$.
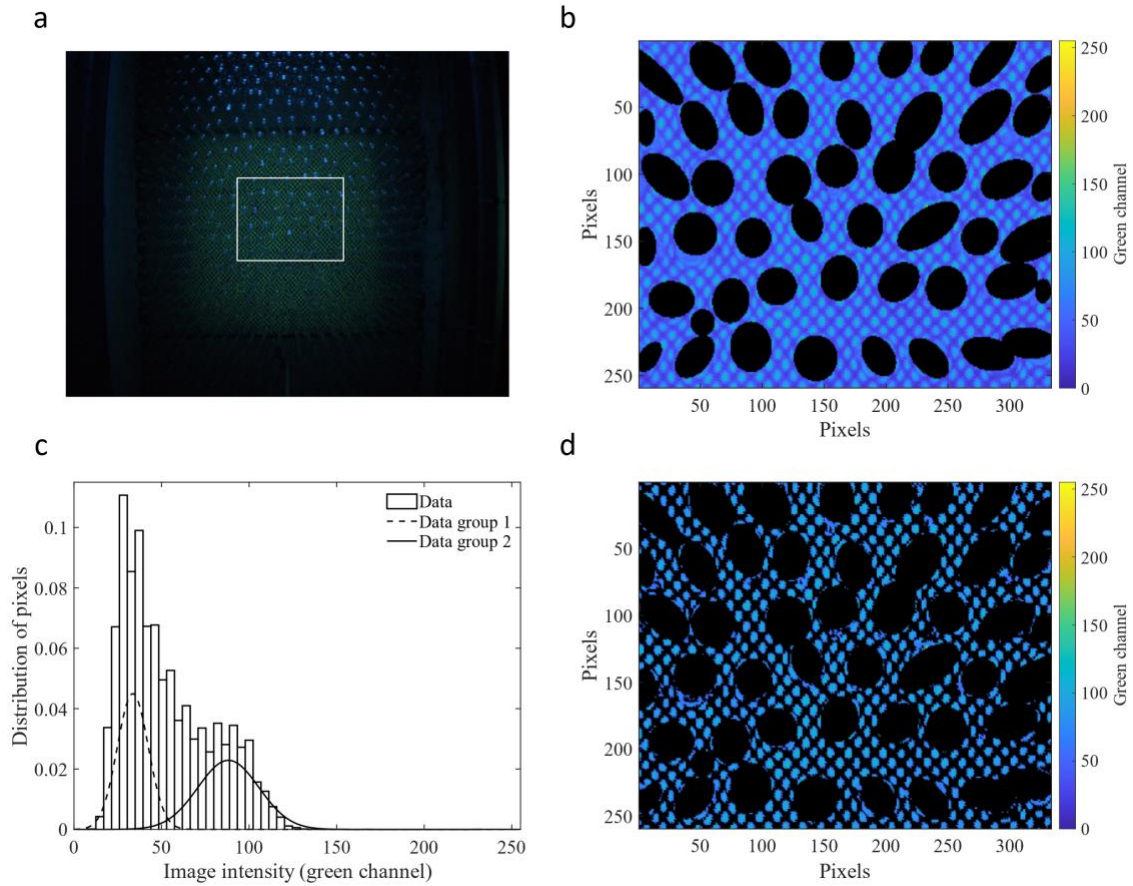

Figure S10. Image processing steps. (a) Crop the original image. (b) Remove the pixels occupied by vegetation dowels. (c) Separate pixels into two groups. (d) Locate the pixels occupied by hydrogel beads and pore water.

8
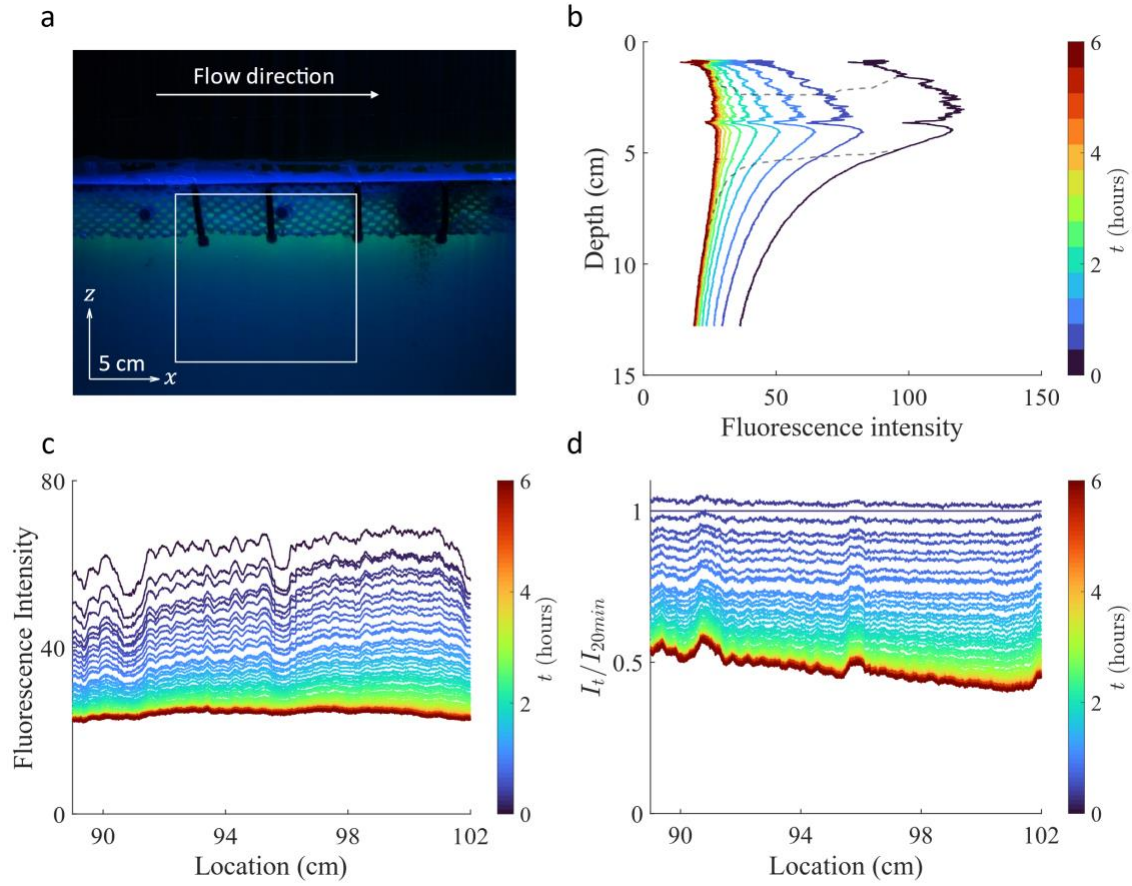
Figure S11. Dye release experiment captured by a side-looking camera. (a) The dye distribution at the beginning of the experiment. The fluorescent dye (green) was injected at 0 cm to 5 cm below the sediment surface. The fluorescence signal below 8 cm was due to the light scattered from above. The white box represents the region of interest used in the analyses. The left and right boundaries of the white box are also the boundaries of the region in the dye release experiments captured by a downward-looking camera (Fig S10a). (b) Vertical distribution of fluorescence intensity (averaged along x-axis). The line color presents experimental time with 30-minute intervals. Region between two gray dash lines show the region where fluorescence intensity exceeds 80% peak fluorescence intensity for each profile. (c) Streamwise distribution of fluorescence intensity (averaged along z-axis) with 5-minute time interval between lines. I_t stands for the fluorescence intensity at time t. (d) Streamwise profiles in (c) normalized by profile at t = 20 minutes.
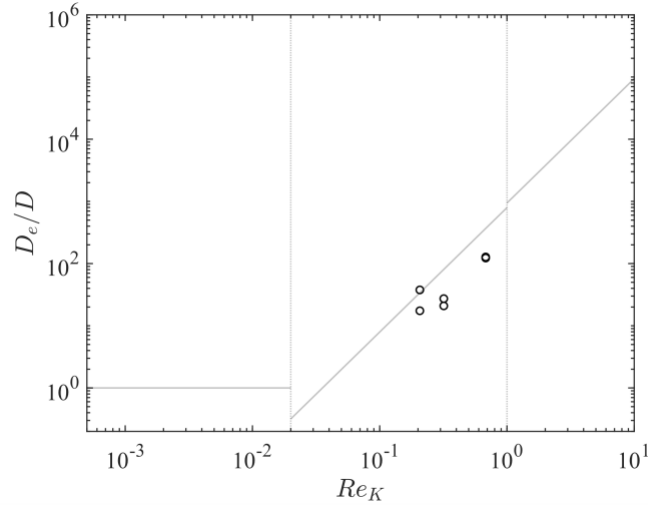
Figure S12. The normalized effective diffusion coefficient D_e/D and the permeability Reynolds number Re_K of cases without vegetation. D is molecular diffusion coefficient of 2.0×10^{-9} m^2/s when water is 20℃. $Re_K = K^{0.5}u_*/\nu$. K is the sediment permeability. u_* is the shear velocity and ν is the fluid kinematic viscosity. Effective diffusion coefficient D_e is evaluated by Eq. 20 of Grant et al. (2012). Gray lines are the interfacial transport model proposed by Voermans et al. (2018a). The circles are our measurements of the cases without vegetation. Note that the friction velocity used to calculate Re_K was estimated by fitting the vertical flow velocity profile with log velocity profile. The flow in the cases with mean flow velocity of 1.7 cm/s is transitional flow ($Re = 1973$) and its velocity profile doesn't follow log profile, thus, the friction velocities cannot be estimated, and the data are not shown in the plot.

Table S1. Flow conditions and effective diffusion calculated using 1D diffusion model of each case. Friction velocity u_* was estimated by fitting vertical velocity profiles with log profile. Vegetation Reynolds number Re_v was calculated with the modified vegetation-related hydraulic radius following Cheng and Nguyen (2011). Permeability Reynolds number Re_K and turbulent shear penetration depth δ_p were calculated using the formulated proposed by Voermans et al. (2018a). Effective diffusion coefficient D_e is evaluated by Eq. 20 of Grant et al. (2012).

	U [m/s]	u_* [m/s]	Re	$Re_v{}^*$	$Re_K{}^{**}$	$\delta_p{}^{***}$ [m]	D_e [m^2/s]	V_H [m/s]
	0.017	-	1793	-	-	-	2.5E-08	7.2E-07
	0.017	-	1793	-	-	-	1.2E-08	1.2E-06
	0.040	0.0024	4344	-	0.21	0.00022	3.5E-08	1.8E-06
Cases without vegetation	0.040	0.0024	4344	-	0.21	0.00022	7.6E-08	1.1E-06
	0.066	0.0037	7107	-	0.32	0.00031	5.5E-08	1.4E-06
	0.066	0.0037	7107	-	0.32	0.00031	4.2E-08	1.4E-06
	0.154	0.0079	16524	-	0.68	0.00058	2.6E-07	4.1E-06
	0.154	0.0079	16524	-	0.68	0.00058	2.5E-07	3.8E-06
	0.007	-	844	471	-	-	1.9E-08	5.7E-07
	0.007	-	844	471	-	-	6.2E-09	5.5E-07
	0.016	-	1793	1002	-	-	4.6E-08	1.5E-06
Cases with vegetation	0.016	-	1793	1002	-	-	4.0E-08	1.3E-06
	0.024	-	2636	1473	-	-	8.5E-08	2.5E-06
	0.024	-	2636	1473	-	-	7.3E-08	2.7E-06
	0.036	-	4007	2239	-	-	1.6E-07	3.5E-06
	0.036	-	4007	2239	-	-	8.7E-08	4.0E-06

* $Re_v = U r_v / \nu$, where $r_v = \dfrac{\text{water volume}}{\text{effective wetted area}} = \dfrac{8 d s^2 H}{3 d_v H}$

** $Re_K = \sqrt{K} u_* / \nu$; K is the sediment permeability; u_* is the shear velocity and ν is fluid kinematic viscosity.

*** $(\delta_p u_*)/\nu \approx 8 Re_K^{1.8}$.